Multistep excitation of autoionizing Rydberg states

N. H. Tran, P. Pillet,* R. Kachru, and T. F. Gallagher
Molecular Physics Laboratory, SRI International, Menlo Park, California 94025
(Received 28 November 1983)

We describe the photoexcitation spectra from bound Ba Rydberg states $6snl$ to the analogous autoionizing $6pnl$ states. The spectra are obtained with high laser power bringing out weak spectral features corresponding to changes in n of the outer nl electron. These spectra are explained using a quantum-defect-theory approach which shows that the optical cross section is a product of the spectral density of the autoionizing states and the overlap integral from the initial bound state. When a saturation effect is taken into account, synthetic spectra calculated in this way accurately reproduce the observed spectra. Experimental spectra of unperturbed autoionizing series are presented together with the two-channel quantum-defect theory relevant to this case. In addition, the new features which arise in the case of interacting series are shown as well as a model three-channel quantum-defect-theory treatment.

I. INTRODUCTION

Several years ago Cooke *et al.*[1] introduced a method of multistep laser excitation of autoionizing states of alkaline-earth atoms. A central feature of the technique is that one electron is excited at a time, which leads to two very attractive features. First, since each electron is excited separately it is relatively straightforward to assign the transitions. Second, the choice of final transition to the autoionizing state leads only to excitation of a single autoionizing state but not the continuum. In Ba, typically an intermediate bound $6snl$ Rydberg state is excited followed by the final transition to an analogous $6pnl$ autoionizing Rydberg state converging to the excited $6p$ state of the ion. Under these circumstances the excitation spectrum usually consists of a single Lorentzian feature which yields directly the position and width of the autoionizing $6pnl$ state in contrast to the Beutler-Fano interference profile commonly associated with autoionizing states.[2]

In recent observations, with higher laser power, more complex spectra have been obtained. Specifically, broadening of the central feature associated with the $6pnl$ state and additional very asymmetric features corresponding to Rydberg states of different n have been observed. These observations cannot be easily explained using the picture as originally presented by Cooke *et al.*[1] However, using the physical insights derived from this simple picture as a guide, it is possible to calculate the optical excitation cross sections using quantum-defect theory. Using the cross sections calculated in this fashion and taking into account the saturation effects produced by the high laser flux described by Cooke *et al.*[3] it is possible to calculate synthetic spectra which reproduce very well the observed spectra. A short account of this has already been given by Tran *et al.*[4] for the case of an unperturbed series of autoionizing states. Here, we present a complete description of the calculations for this case, which may be treated by two-channel quantum-defect theory, as well as additional experimental examples. We also present additional data which illustrate new features which arise when there are two interacting Rydberg series of autoionizing states. These effects are shown to be in qualitative agreement with calculations based on a three-channel quantum-defect model.

In Sec. II we review the basic physical notions of the multistep excitation and describe the experimental approach. Then, in Sec. III, the two-channel case, relevant to an unperturbed series of autoionizing states, is treated in detail, and the variety of spectra which may be obtained even in this simple case is illustrated. Subsequently, in Sec. IV, the three-channel case, two interacting Rydberg series converging to two limits, is considered as well as examples of new phenomena which occur in this case. Finally, in Sec. IV, the potential extensions and usefulness of the method as a tool are discussed.

II. BASIS OF THE APPROACH, EXPERIMENTAL METHOD, AND TYPICAL OBSERVATIONS

Let us consider the excitation of the bound Ba $6s15d$ state to the autoionizing $6p15d$ state and nearby states as an example. (For the moment we ignore the spin of the electrons to simplify the notation.) Ba atoms are excited to the $6s15d$ state by two dye-laser pulses as shown by the energy-level diagram of Fig. 1. Subsequently, a third laser drives the Ba^+ $6s$-$6p$ transition to the autoionizing $6p15d$ Rydberg state. Each atom excited to the autoionizing state quickly decays and the resulting ions are detected as the wavelength of the third laser is scanned. Why this approach leads to a simple spectrum is apparent when we consider what the successive laser pulses do to the atom. The first and second lasers excite one of the electrons to the bound $6s15d$ Rydberg state in which the electron is usually far from the ionic core. The third laser excites the $6s$-$6p$ transition of Ba^+ while the outer electron is a spectator. The most likely result is that the outer electron will remain in the $15d$ state in which case scanning the third laser across the $6s15d$-$6p15d$ transition yields immediate-

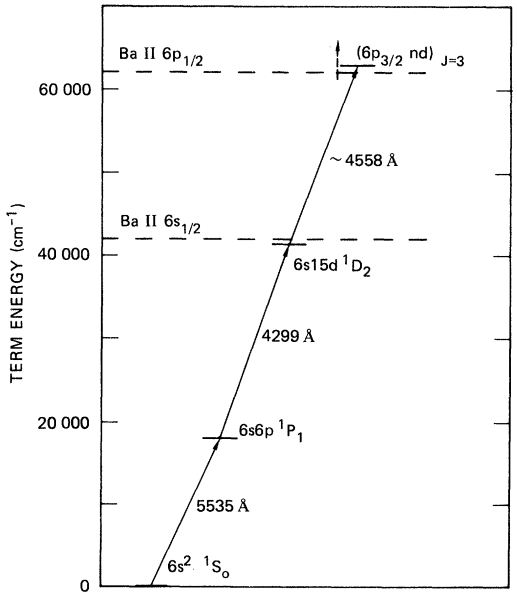

FIG. 1. Ba energy levels showing the three laser pumping steps.

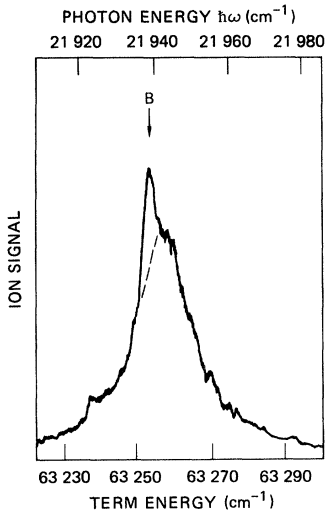

FIG. 2. Low-power scan of the third laser across the Ba $6s15d\,^1D_2 \rightarrow (6p_{3/2}15d_j)_{J=3}$ transition taken with all three lasers circularly polarized in the same sense. This scan yields the position and width of the $(6p_{3/2}15d)_{J=3}$ state. Narrow peak denoted by B is a coincidence (see Table I). Term energy of the $6s15d$ state is 41 315.5 cm^{-1}.

ly the position and width of the $6p15d$ state. However, there is a small, but finite, chance of the outer electron making a readjustment in its orbit allowing the transitions to neighboring $6pnd$ states. Finally, we note that although the direct photoionization of the $6s15d$ state to the $6s\epsilon p$ or $6s\epsilon f$ continua is possible it is unlikely. This is so because at the large orbital radius, $\simeq$100 Å, where the $15d$ electron is most likely to be found, the spatial oscillations of the $15d$ radial wave function are much less rapid than those of the 2.4-eV continuum wave function which would result from photoionization. Thus there is negligible continuum excitation, and the possibility of discrete-continuum interference which leads to the familiar Beutler-Fano profile is effectively absent.

Since the details of the apparatus and approach have been described elsewhere,[1] we only recount the major features here. The atomic beam of Ba effuses from a resistively heated oven and passes between a plate and a grid 1.1 cm apart where it is crossed by the three sequentially pulsed dye-laser beams. Subsequent to the laser pulses a 50-V pulse is applied to the plate driving any ions resulting from the excitation and subsequent decay of an autoionizing state to a particle multiplier, the output of which is recorded with a gated integrator.

The three dye lasers are all pumped by harmonics of the same Nd:YAG laser, and the second and third laser beams are delayed so the three laser pulses are sequential in time. The laser pulse lengths are $\simeq$5 ns, and the pulse energies are $\simeq$100 μJ. With beam diameters of 1 mm, this leads to integrated fluxes of 10^{15} photons/cm^2. In addition to recording the atomic spectrum, as the third laser is scanned its power and frequency are recorded by monitoring the transmission through a 3.52-cm^{-1} free spectral range (FSR) Fabry-Perot etalon with a photodiode.

If we scan the wavelength of the third laser in the vicinity of the Ba $6s15d$-$6p15d$ transition we observe with low laser power an ion signal as shown in Fig. 2. Specifically, Fig. 2 is a recording of the $6s15d\,^1D_2 \rightarrow (6p_{3/2}15d_j)_{J=3}$ transition taken with all three lasers circularly polarized to ensure that only the $J=3$ state is populated. As shown by Fig. 2 the signal is a single feature which is proportional to the optical absorption cross section, or oscillator strength, and has a Lorentzian line shape. The center of the feature gives the location of the $6p_{3/2}15d$ state and its width the total autoionization rate. As shown by Fig. 2 the center of the observed feature lies near the Ba^+ $6s_{1/2} \rightarrow 6p_{3/2}$ ion line at 21 953 cm^{-1}. The frequency difference from the frequency of the ion line immediately tells us the difference in quantum defects of the $6s15d$ and autoionizing $6p_{3/2}15d$ states. In Fig. 2 there is a two-photon marker line, indicated by B, which arises from the resonant absorption of two photons from the third laser by an atom in the $6s6p$ state. Specifically, one photon drives the transition to the higher-lying $6s10d\,^1D_2$ state and the second drives the transition to the autoionizing $6p_{3/2}10d$ state. This and other marker lines, which occur at known wavelengths,[5,6] comprise a useful set of frequency markers. In Table I we tabulate the marker lines, labeled by letters, which occur in the experimental spectra presented in this paper.

In the limit of low laser flux the detected ion signal is proportional to the optical cross section. At higher laser flux we must take into account the effect termed "depletion broadening" by Cooke *et al.*[3] For any power the detected signal may be generally expressed as

$$I = I_0(1 - e^{-\sigma\phi}) , \tag{1}$$

where I_0 is the number of atoms in the bound Rydberg state, σ is the optical cross section, and ϕ is the integrated laser flux. Here we ignore the possibility of driving transitions back and forth between the two states. From Eq. (1) it is clear that the maximum signal is I_0 and that the

TABLE I. Markers lines in the spectra.

Designation	λ_{meas} (Å)	Transition $6s6p\,^1P_1 \rightarrow$	$\hbar\omega$ (cm^{-1})
A	4512	$6s10d\,^3D_2$	22 163.1
B	4557	$6s10d\,^1D_2$	21 938.1
C	4574	$6s10d\,^3D_2$	21 861.9
D	4627	$6s11s\,^1S_0$	21 661.6
E	4673	$5d8s\,^1D_2$	21 404.7
F	4699	$6s9d\,^1D_2$	21 274.6
G	4739	$6s9d\,^3D_2$	21 097.7
H	4792	$6s10s\,^1S_0$	20 863.6
I	4853	$6s10s\,^3S_1$	20 603.5
J	4879	$6s8d\,^1D_2$	20 495.0
K	4948	$5d6d\,^3P_2$	20 207.4

signal is only proportional to the optical cross section in the limit $\sigma\phi \ll 1$. In these experiments the peak optical cross section is $\sim 10^{-13}$ cm^2 (at 21 945 cm^{-1} in Fig. 2), and the maximum available laser flux is $\sim 10^{15}$ photons/cm^2. Thus even where the cross section has decreased by a factor of 100 it is possible to see a signal approaching I_0. This produces a broadening of the observed signal which led to the name applied by Cooke *et al.*[3] An example of such a signal is shown in Fig. 3 which is a recording of the same transition shown in Fig. 2 with higher laser flux. For later use we define a saturation factor $N = \sigma_m \phi$, where σ_m is the maximum of the cross section. In Fig. 3 $N \sim 100$.

In Fig. 3, the broadening implied by Eq. (1) is quite evident as is the presence of very asymmetric satellite features which correspond to Rydberg states of other *n*. In fact, spectra such as the one shown in Fig. 3 can be accounted for in a very straightforward fashion, as shown in Sec. III.

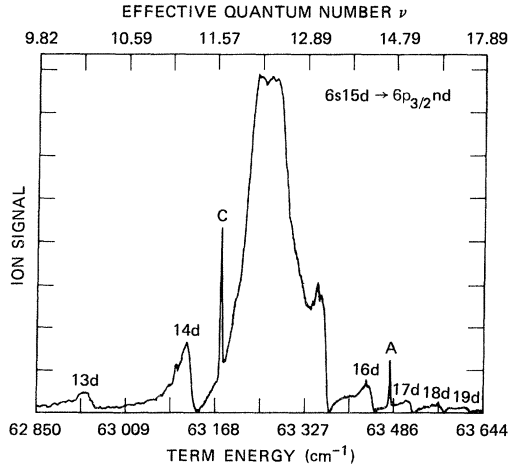

FIG. 3. A high-power scan of the third laser in the region of Ba $6s15d\,^1D_2 \rightarrow (6p_{3/2}15d_j)_{J=3}$ transition. Note the asymmetric satellite features corresponding to other $6p_{3/2}nd$ states. Power of the third laser is 50 times higher than in Fig. 2. Marker lines denoted by letters are tabulated in Table I.

III. AN UNPERTURBED SERIES OF AUTOIONIZING STATES: A TWO-CHANNEL CASE

Let us consider the specific problem illustrated by Fig. 4, in which we have the unperturbed series of $(6p_{3/2}nd)_{J=3}$ states converging to the $6p_{3/2}$ limit of Ba^+. These autoionizing states are degenerate with 13 continua of the same *J* which are represented by one continuum *X*. This is a good approximation in this particular case because the only role of the continua is as a sink for the products of autoionization. Below the $6s_{1/2}$ limit is a bound Rydberg state $6snd$ of even parity from which we excite to the odd-parity $6p_{3/2}nd$ autoionizing Rydberg states.

To a first approximation we may consider each of the autoionizing states to be slightly broadened so that its character is spread over a small energy range. This point of view is quite adequate to explain observations such as the one shown in Fig. 2 in which only one feature is observed. However, it is not easily generalized to explain observations such as Fig. 3 in which the observed spectrum is essentially continuous from one feature to the next and covers a range of *n* states.

To deal with spectra such as the one shown in Fig. 3 we have adopted a quantum-defect-theory[4] approach to characterize the autoionizing states. The details of a two-channel analysis are given by Fano in his treatment of H_2 (Ref. 7) so we here concentrate on the extension of those results to our problem. A central notion of quantum-defect theory is that the non-Coulombic interaction of the outer electron with the core occurs at very small orbital radius which leads to an $r \rightarrow 0$ boundary condition, while as $r \rightarrow \infty$ the electron experiences a purely Coulomb potential which imposes a second boundary condition. It is thus not surprising that the atomic wave function can be expressed in terms of either the close-coupled states more characteristic of small *r* or the collision channels more characteristic of large *r*. In an atom with two valence electrons these channels are usually *LS* and *jj* coupled, respectively. In the excitation of autoionizing states from the ground state both electrons are ini-

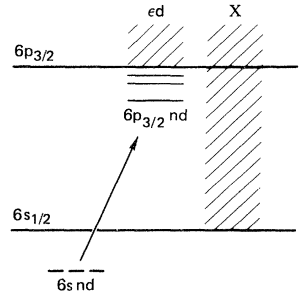

FIG. 4. Schematic levels for a two-limit problem. The two ionization limits are shown as well as the Rydberg series (——) and the continua (///). A bound state of opposite parity from which the excitation occurs is also shown (— — —). Excitation from the bound to the autoionizing Rydberg state is shown by the arrow.

tially at small r and the excitation process is appropriately described using the close-coupled channels. Historically this has been the most common experimental approach, and thus the theoretical work has been focused on this problem. However, in our case in which the outer electron is at large orbital radius during the excitation to the autoionizing state it is appropriate to describe the excitation in terms of the collision channels. Thus we choose to represent the wave function in terms of the collision channel expansion. Since the role of the continua is only to provide a sink for ejected electrons, we represent all the continua by the continuum X which we label channel 1. We label the series of discrete nd autoionizing states converging to the $6p_{3/2}$ limit as channel 2. This is shown in Fig. 4 where the continuum X is shown above the $6s_{1/2}$ limit for concreteness. With this notation we may represent the wave function for a state of specific parity, angular momentum, and energy E in the autoionization region as

$$\Psi_A = Z_1 \chi_1 \Phi_1 C(l,\gamma,r,\tau) + Z_2 \chi_2 \Phi_2 C(l,\nu,r) \ . \tag{2}$$

Here χ_i and Φ_i represent the wave functions of the ion core and the angular part of the outer electrons' wave function, respectively, for the two channels. We take each of these χ and Φ functions to be independently normalized to 1. The functions $C(l,\gamma,r,\tau)$ and $C(l,\nu,r)$ represent continuum and bound Coulomb wave functions for an electron of angular momentum l and radial position r. The continuum function is also characterized by the energy γ of the electron relative to its ionization limit and its phase shift $\pi\tau$ (relative to a hydrogenic wave function). We note that if the continuum entered into the problem in a way other than merely as a sink for electrons, we would need to specify its phase shift and ionization limit. The bound Coulomb wave function needs only the effective quantum number ν for both the energy and phase shift since for a given phase shift only one value of ν (mod 1) is allowed. The effective quantum number ν is defined by

$$E = I_2 - 1/2\nu^2 \ , \tag{3}$$

where I_2 is the energy of the second ionization limit and E is the total energy represented by the wave function. In the above equation and throughout this paper we use atomic units. E is of course related to γ by

$$E = I_1 + \gamma \ . \tag{4}$$

The continuum Coulomb wave functions are normalized per unit energy and the bound-state wave functions are normalized so that the bound and continuum wave functions for $E \to I_2$ of the same l and τ are identical. As a consequence of this, for the bound-state wave functions $|\langle C(l,\nu,r)\,|\,C(l,\nu,r)\rangle| = \nu^3$, that is, the normalization differs from that of the ususal bound-state radial wave functions by a factor of $\nu^{3/2}$.

Note that the Coulomb wave functions themselves tell us nothing about the structure of the autoionizing region, they only tell us what the continuum and bound part of the wave functions look like. The information about the structure comes from the weightings Z_1^2 and Z_2^2. If we follow the usual convention that a continuum wave function should be normalized per unit energy then $Z_1^2 \equiv 1$, for as $r \to \infty$ the bound channel 2 part of the wave function vanishes. Thus the continuum (channel 1) amplitude is structureless. Z_2 represents the amplitude of channel 2 per unit energy and is derived from quantum-defect theory. Z_2 is a function periodic in ν given by[7]

$$Z_2 = (\partial\tau/\partial\nu)^{1/2} \ . \tag{5}$$

In Fig. 5 we show as an example the plot of τ vs ν (mod 1), conventionally called a Lu-Fano[8] plot, appropriate to the Ba $(6p_{3/2}nd)_{J=3}$ states.[9] As implied by Eq. (5), Z_2^2 is simply the slope of the Lu-Fano plot and is shown in Fig. 6 plotted versus ν (mod 1). Figure 6 corresponds to the profile of the autoionizing state, the location of which corresponds to the region of the phase shift of the continuum shown in Fig. 5, as expected from more conventional configuration-interaction treatments.[2] For simplicity we shall define the value of ν at the center of the Z_2^2 profile as the effective quantum number of the autoionizing state which we shall label n_A. We shall use n with no subscript only as an integer to label states. On the other hand, n with a subscript will be used to denote fixed, usually noninteger, values; and ν with or without subscripts as a continuous variable. We denote the full width at half maximum of the autoionizing state by Γ. Thus from Fig. 6, it is apparent that for the $(6p_{3/2}nd)_{J=3}$ states $n_A = n - 2.75$ and $\Gamma = 0.11\nu^{-3}$. Recall that a change of 1 in ν corresponds to a change in energy of ν^{-3}. It is useful to express the width as a fraction of the energy spacing between successive members of the series; i.e., the fractional width $\bar{\Gamma} = \Gamma\nu^3$ [$\Gamma = 0.11$ for the $(6p_{3/2}nd)_{J=3}$ states].

As noted above, Z_2 only depends on the slope of the Lu-Fano plot, the continuum phase shift, and not at all on the phase. Thus a Lu-Fano plot offset vertically from Fig. 5 would lead to the same dependence of Z_2 although the quantum-defect parameters, and other atomic properties, would be completely different. This arbitrariness is a direct consequence of the fact that Z_2^2, the spectral density of the autoionizing state, is insensitive to the phase of the open channel, which serve only as a sink for electrons

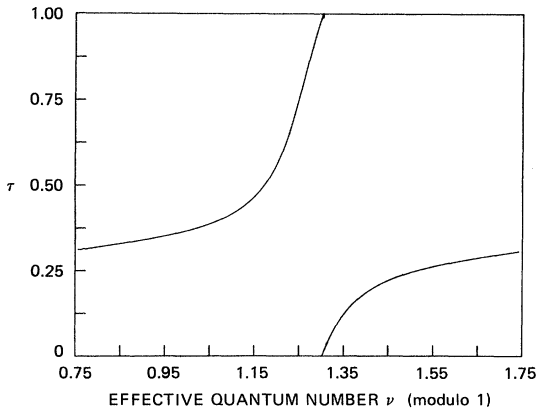

FIG. 5. A plot of τ, the phase shift in the open channel divided by π, as a function of the effective quantum number ν.

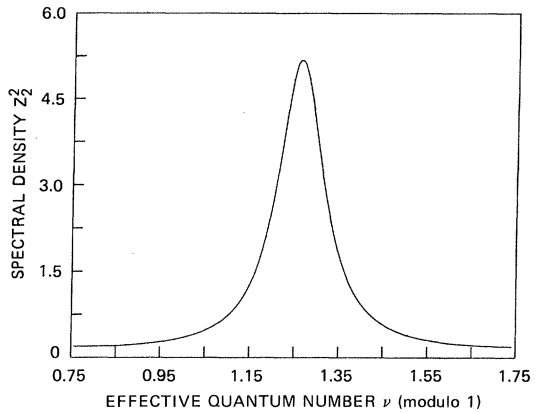

FIG. 6. Derivative vs ν of Fig. 5, which is the spectral density Z_2^2.

ejected in the autoionization of the discrete states.

For our two-channel treatment of the $(6p_{3/2}nd_j)_{J=3}$ states interacting with one continuum we choose as the collision channels 1 and 2, the continuum X and $6p_{3/2}nd_{3/2}$, and as the close-coupled channels 1 and 2, Λ and Ω. These labels for the close-coupled channels are chosen to emphasize the fact that their only function is to connect the open and closed collision channels. The eigenquantum defects μ_1 and μ_2 of the two close-coupled channels are 0.30 (mod 1) and 0.75 (mod 1), respectively. The i collision channel may be expressed in terms of the α collision channels by the $U_{i\alpha}$ rotation matrix

$$U_{i\alpha}=\begin{bmatrix}\cos\theta & \sin\theta\\ -\sin\theta & \cos\theta\end{bmatrix} . \tag{6}$$

In Fig. 5 we have used $\theta=0.42$ rad. Since there are only two experimental parameters n_A and Γ which characterize the positions and widths of the $6p_{3/2}nd_j$ series, it is evident that there is some degree of arbitrariness in how we choose the three quantum-defect parameters μ_1, μ_2, and θ. We have taken advantage of this arbitrariness and have chosen the quantum-defect parameters of Fig. 5 so that the interaction strength is mostly contained in the rotation matrix of Eq. (6) connecting the close-coupled and collision channels. We note that this arbitrariness is removed if we parameterize the $6p_{3/2}nd_j$ series in terms of n_A and Γ as has been done recently by Cooke[10] rather than by μ_1, μ_2, and θ.

To describe the excitation from the bound Rydberg state to the autoionizing state we return to our physical picture of driving the ion core transition with the outer electron remaining a spectator at a large orbital radius. This picture has already led us to express the wave function in terms of the collision channels and not the close-coupled channels which would be appropriate for excitation from the ground state. The physical picture also suggests how to explicitly represent the excitation.

First, recalling that there is no direct continuum excitation, we only need to consider excitation to the bound channel 2 of Eq. (2). Thus we need to calculate the dipole matrix element between the initial bound state and the bound channel 2 portion of the wave function in the autoionizing region. The initial bound state Ψ_B may be represented in the same manner as the bound part of Eq. (2), i.e.,

$$\Psi_B=Z_B\chi_B\Phi_B C(l_B,n_B,r) . \tag{7}$$

Z_B is a product of a δ function in energy $\delta(E-E_B)$ and a factor of $\nu_B^{-3/2}$, i.e., $Z_B=\delta(E-E_B)\nu_B^{-3/2}$, which specifies the initial bound state as having a well-defined energy and the more conventional normalization $\langle\Psi_B\,|\,\Psi_B\rangle=1$. Recall that the Coulomb radial wave functions $C(l,n_B,r)$ are normalized per unit energy. The functions χ_B and Φ_B include the $6s$ ion core wave functions and angular parts of the outer electron wave function just as in Eq. (2).

Our original notion that the transition is essentially one of the ion core with the outer electron a spectator suggests that we write the dipole matrix element $\langle\Psi_B\,|\,\mu\,|\,\Psi_A\rangle$ in terms of the dipole matrix element for the ion core transition and an overlap integral for the outer electron. Specifically, we write the electric dipole transition matrix element from the bound Rydberg state Ψ_B to the autoionizing state Ψ_A as

$$\langle\Psi_B\,|\,\mu\,|\,\Psi_A\rangle=Z_BZ_2\langle\chi_B\,|\,\mu\,|\,\chi_A\rangle\langle\Phi_B\,|\,\Phi_2\rangle \times\langle C(l_B,n_B,r)\,|\,C(l,\nu,r)\rangle . \tag{8}$$

If we examine the factors on the right-hand side of Eq. (8), we see first the spectral densities Z_B and Z_2. The dipole matrix element of the ion core transition is given by $\langle\chi_B\,|\,\mu\,|\,\chi_A\rangle$. The angular factors of the outer electron wave functions for the bound and autoionizing states are given by $\langle\Phi_B\,|\,\Phi_2\rangle$ which implies that a bound state with an outer electron in a state of angular momentum l is only connected to an autoionizing state of the same angular momentum. It also contains factors of order 1 for jj-LS recoupling. For our purposes it is adequate to represent it by a Kronecker δ function; $\langle\Phi_B\,|\,\Phi_2\rangle=\delta_{l_Bl}$. Finally, we have the overlap factor of the bound and continuum wave functions $\langle C(l_B,n_B,r)\,|\,C(l,\nu,r)\rangle$. Recalling that l_B must equal l by virtue of the angular factors we may introduce the shorthand $O(l,n_B,\nu)=\langle C(l,n_B,r)\,|\,C(l,\nu,r)\rangle$. We know that $O(l,n_B,n_B)=n_B^3$ and $O(l,n_B,n_B\pm i)=0$ for i an integer different from zero due to orthonormality of the wave functions. In fact, it is an oscillating function for which an approximate analytic expression which does not depend on l has been derived by Bhatti *et al.*[11] Explicitly their expression may be rewritten as

$$O(l,n_B,\nu)\cong\frac{2n_B^2\nu^2}{n_B+\nu}\frac{\sin[\pi(\nu-n_B)]}{\pi(\nu-n_B)} . \tag{9}$$

Note that Eq. (9) differs from the expression of Bhatti *et al.*[11] by a factor of $(n_B\nu)^{1/3}$ which reflects the different normalizations of the wave functions. One may obtain $O(l,n_B,\nu)$ from Eq. (9) or calculate it numerically in a straightforward fashion.[11,12] The cross section is given by[13]

$$\sigma=\frac{4\pi^2\omega}{c}|\langle\Psi_B|\mu|\Psi_A\rangle|^2$$
$$=\frac{4\pi^2\omega}{c}Z_B^2Z_2^2|\langle\chi_B|\mu|\chi_A\rangle|^2|\langle\Phi_B|\Phi_2\rangle|^2$$
$$\times|\langle C(l,\nu,r)|C(l,n_B,r)\rangle|^2, \quad (10)$$

where ω is the angular frequency of the incoming photon and c is the speed of light ($c=137$ in atomic units). Let us collect the constant or nearly constant factors of Eq. (10). First we recognize that $\omega|\langle\chi_B|\mu|\chi_A\rangle|^2=\frac{1}{2}f_{\rm ion}$ where $f_{\rm ion}$ is the oscillator strength of the Ba^+ $6s$-$6p$ transition, which is calculated to be 1.16.[14] Thus Eq. (10) may be written

$$\sigma=\sigma_0Z_B^2Z_2^2O^2(l,n_B,\nu) \quad (11)$$

where $\sigma_0=2\pi^2f_{\rm ion}|\langle\Phi_B|\Phi_2\rangle|^2/c$. Assuming that $|\langle\Phi_B|\Phi_2\rangle|^2=1$ and $f_{\rm ion}=1.16$ we find that $\sigma_0=0.167a_0^2$ or 0.047 Å^2.

It is useful to evaluate the cross section at is maximum, σ_m. In most cases the quantum defects of the bound and autoionizing states are very nearly equal, so that $n_A\approx n_B$ in which case $O^2(l,n_B,\nu)=n_B^6$. Since $Z_B^2=n_B^{-3}$, together these two factors yield an n_B^{+3} scaling for the cross section. Recalling that Z_2^2 is given by the slope of the Lu-Fano plot it is apparent that the maximum value of $Z_2^2\sim1/\overline{\Gamma}$. In fact, approximating the shape of the autoionizing state by a Lorentzian leads to a maximum value of $Z_2^2=2/\overline{\Gamma}$.

Collecting all these terms it is evident that

$$\sigma_m=2\sigma_0\frac{n_B^3}{\overline{\Gamma}}. \quad (12)$$

For our example of the $6s15d\,^1D_2\rightarrow6p_{3/2}nd$ spectrum for which $n_B=12.35$ (Ref. 6) and $\overline{\Gamma}=0.11$,[9] numerical evaluation of Eq. (12) yields $\sigma_m=1.6\times10^3$ Å^2. Thus an integrated laser flux of 10^{15} cm^{-2} leads to $N\sim100$.

From Eq. (11) it is clear that the energy dependence of the cross section is mainly contained in Z_2^2, the density of the autoionizing states, and $O^2(l,n_B,\nu)$, the square of the overlap integral. Bizarre spectra such as Fig. 3 occur because the maxima in Z_2^2 nearly coincide with the zeros in the overlap integral. In Fig. 7 we show plots of Z_2^2, $O^2(l,n_B,\nu)$, and their product which is proportional to the optical cross section. In calculating $O(l,n_B,\nu)$ we have used the fact that for the bound $6s15d\,^1D_2$ state $n_B=12.35$.[6] As shown by Fig. 7, the decrease in $O(l,n_B,\nu)$ away from $\nu\approx n_B$ coarsely restricts the dominant part of the cross section to the central lobe $|\nu-n_B|<1$. Within the central lobe it is the variation of Z_2 which leads to the observed structure in the cross section. Thus, for reasonably narrow autoionizing states the cross section strongly resembles Z_2^2, which as we noted before fully describes the position and width of the autoionizing states. Furthermore, Eq. (12) indicates that the peak value of the cross section, at the center of the autoionizing state where $\nu=n_A\approx n_B$, is proportional to n_B^3. However, the width Γ of the autoionizing state is proportional to n_A^{-3} so the cross section integrated over the width of the autoionizing state is a constant. Stated another way, the cross section of the Ba^+ resonance line is spread over the width of the autoionizing state. Thus from this quantum-defect model we recover the simple, physically appealing explanation originally advanced by Cooke *et al.*[1] to explain observations such as Fig. 2.

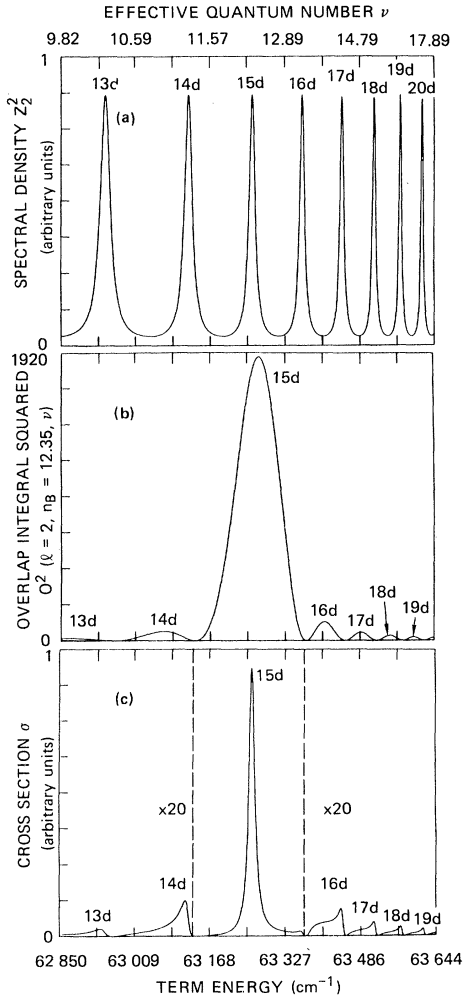

FIG. 7. Plots of (a) the spectral density, (b) the square of the overlap integral between initial and final states, and (c) their product which is proportional to the optical cross section σ. All are calculated for the third laser excitation from the $6s15d$ ($n_B=12.35$) state to the $(6p_{3/2}nd)_{J=3}$ channel.

From Fig. 7 it is apparent that we can only expect to see the weak satellite features corresponding to changing the n of the outer electron with higher flux excitation. Using Eqs. (1) and (11) we may express the signal in terms of the functions Z_2^2 and $O^2(l,n_B,\nu)$ as

$$I=I_0\{1-\exp[-\sigma_0Z_B^2Z_2^2O^2(l,n_B,\nu)N/\sigma_m]\}, \quad (13)$$

where N is the saturation factor defined previously. This allows an immediate comparison with our depletion-broadened spectrum and provides a convenient way to represent the entire cross section. In Fig. 8 we plot the signal implied by the cross section of Fig. 7(c) by using Eq. (13) with $N=100$. From Fig. 8 it is clear that the zeros occur at the points where $\nu=n_B\pm i$ where i is a

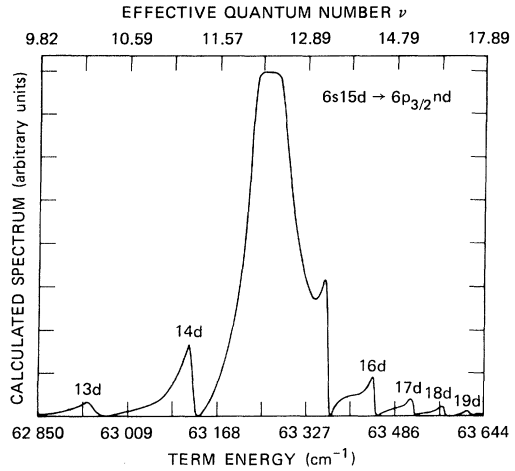

FIG. 8. Calculated spectrum corresponding to Fig. 7(c) for high laser power. Saturation parameter N, defined in the text, is equal to 100.

nonzero integer. Since these points are near the maxima in Z_2^2 the observed signals are very asymmetric. For the case shown in which $n_B > n_A$ the sharp side of the satellite features is to the blue. For the opposite case $n_B < n_A$ the sharp side of the satellite feature is to the red. In the case $n_B = n_A$ only a sharp dip is observed. Finally, in the case $n_B = n_A \pm \frac{1}{2}$ we find two strong features with relatively strong symmetric satellite features. This last case was in fact observed in the original experiments of Cooke *et al.*[1] In Fig. 9 we show the computed cross section σ for a series of autoionizing states of fixed width $\Gamma = 0.11\nu^{-3}$ and $n_B = 12.35$ but various values of n_A. As noted above and as shown by Fig. 9 even a very small change in $n_B - n_A$ can lead to a substantial change in the observed spectrum. We have observed the calculated variation by taking advantage of the variation in effective quantum number of the perturbed bound Rydberg series of Ba. In Fig. 10 we show calculated and observed spectra for the $6s18s \rightarrow 6pns$ and $6s20s \rightarrow 6pns$ transitions which illustrate the reversal of the asymmetry with the sign of $n_B - n_A$.

From the two-channel model and the corresponding experiments, it is clear that the observed spectra depend strongly upon the locations of the autoionizing states and the zeros in the overlap integral. In the excitation of an unperturbed autoionizing series, which may be described by this two-channel model, the relative positions of the zeros and the autoionizing states are fixed for all members of the series, and the observed spectrum is quite regular. On the other hand, if the autoionizing Rydberg series is perturbed so that the locations of the autoionizing states are shifted, this should be quite apparent in the observed

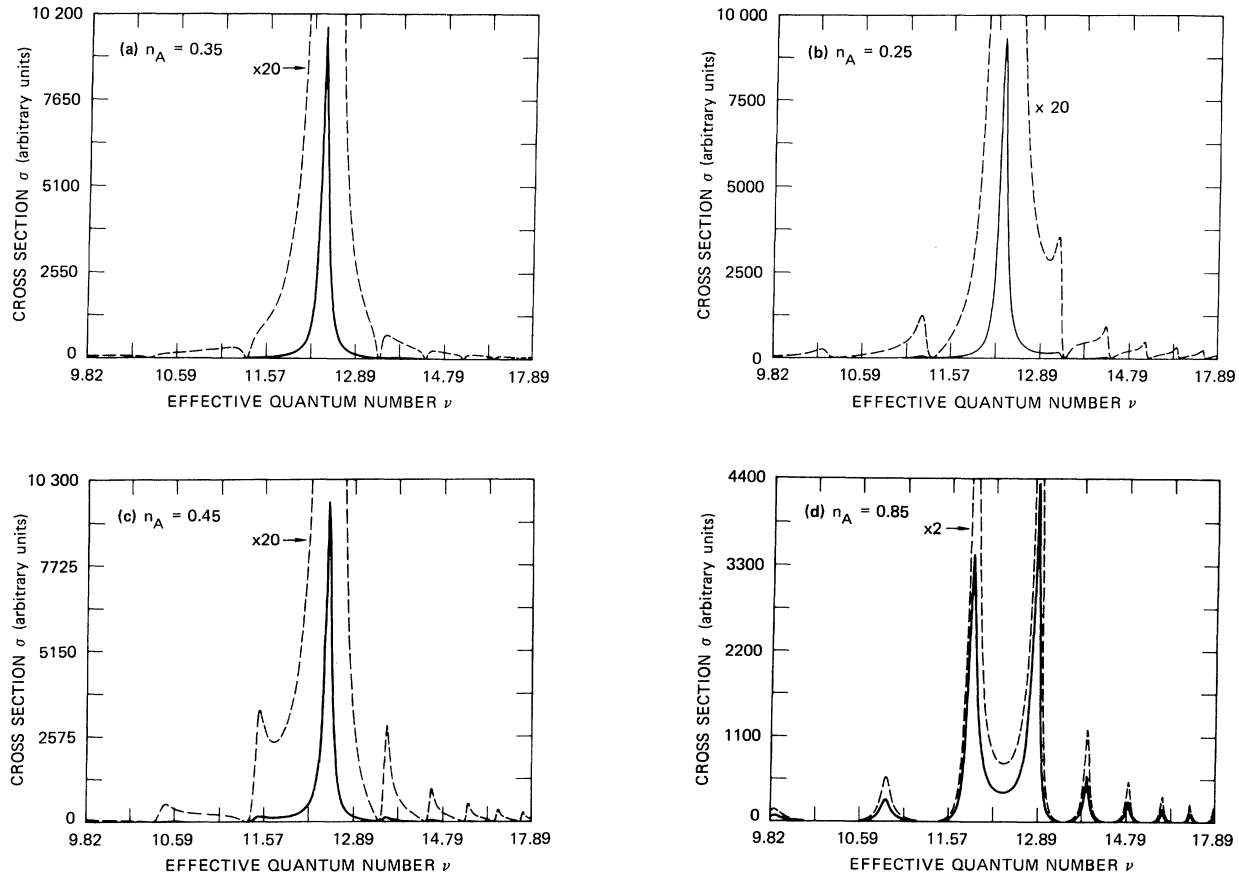

FIG. 9. Calculated cross section σ from a bound state of effective quantum number $n_B = 12.35$ to an autoionizing Rydberg series with $\Gamma = 0.11\nu^{-3}$ and various effective quantum numbers n_A. (a) $n_A = 0.35$, (b) $n_A = 0.25$, (c) $n_A = 0.45$, and (d) $n_A = 0.85$. Note that (b) is the same as Fig. 7(c).

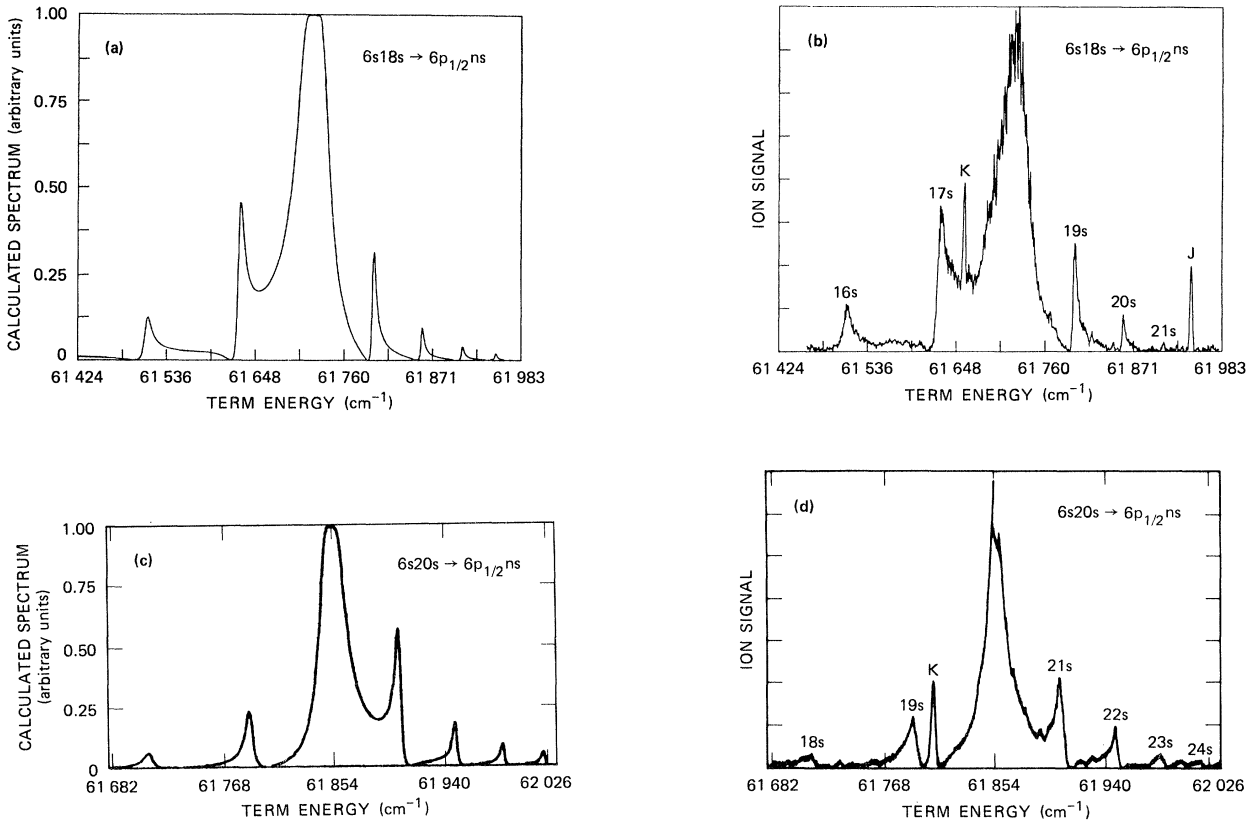

FIG. 10. Calculated and observed spectra obtained for excitation from the $6s18s$ and $6s20s$ states to the $6p_{1/2}ns$ autoionizing states: (a) $6s18s \rightarrow 6p_{1/2}ns$ calculated, (b) $6s18s \rightarrow 6p_{1/2}ns$ observed, (c) $6s20s \rightarrow 6p_{1/2}ns$ calculated, and (d) $6s20s \rightarrow 6p_{1/2}ns$ observed. Marker lines denoted by letters are tabulated in Table I.

spectrum as shown by the sensitivity of the two-channel spectra to the value of $n_A - n_B$. In fact, perturbations of autoionizing series are quite easily observed using this approach, as shown in Sec. IV.

IV. TWO INTERACTING SERIES OF AUTOIONIZING STATES

As we have shown in Sec. III, the excitation spectrum of an unperturbed series of autoionizing states may be reproduced extremely well with a two-channel quantum-defect-theory approach. In this section we consider several new features which arise in the excitation spectra when there are two interacting series of autoionizing states converging to two different ionization limits. Furthermore, we show that these features can be qualitatively understood using a three-channel three-limit quantum-defect theory. The example we shall use consists of the Ba $6pnd$ $J=3$ autoionizing states converging to the $6p_{1/2}$ and $6p_{3/2}$ limits, which are degenerate with continua above the $6s_{1/2}$ and $5d_j$ limits. The two series of autoionizing states, as well as a single continuum X which we shall use to represent all the $6s$ and $5d$ continua, are shown in Fig. 11, as well as the bound $6snd$ state from which the excitation takes place.

The new phenomena which are not present for an unperturbed series of autoionizing states arise from the perturbations in the series regularity by the interseries interaction and from the fact that there are now two possible excitation amplitudes, to the $6p_{1/2}nd$ and $6p_{3/2}nd$ channels.

Let us examine first the consequences of having two excitation amplitudes. Consider the overlap integrals to each of these two $6p_{1/2}nd$ and $6p_{3/2}nd$ channels for two choices of initial states $6s12d$ and $6s23d$. These bound states have effective quantum numbers of 9.356 and

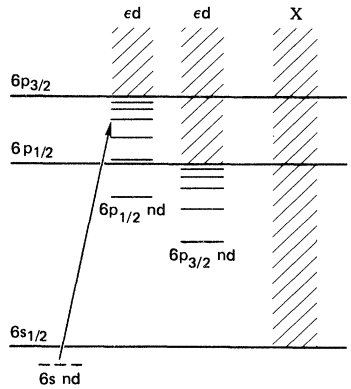

FIG. 11. Relevant levels for a three-channel three-limit treatment of the $6pnd$ levels. Rydberg series converging to each limit are shown (——) as well as the continuum above each limit (///). The bound state of opposite parity is shown (— — —) as well as the excitation to the two channels converging to the $6p_{1/2}$ and $6p_{3/2}$ limits.

20.286, respectively, or equivalently quantum defects $\delta_B = 2.644$ and 2.714, respectively.[6] If ν_2 and ν_3 represent the effective quantum numbers relative to the $6p_{1/2}$ and $6p_{3/2}$ limits and $\pi\tau_2$, $\pi\tau_3$, γ_2, and γ_3 represent phase shifts and energies of the corresponding continuum waves, we can immediately use our previous definition to write the overlap integral from the bound state characterized by n_B and l to the $6p_{1/2}nd$ channel, for example, as

$$O(l,n_B,\nu_2)=\langle C(l,n_B,r) \mid C(l,\nu_2,r)\rangle \ . \tag{14a}$$

Above the $6p_{1/2}$ limit this becomes

$$O(l,n_B,\tau_2,\gamma_2)=\langle C(l,n_B,r) \mid C(l,\tau_2,\gamma_2,r)\rangle \ . \tag{14b}$$

In Fig. 12 we plot these overlap integrals from the $6s12d$ and $6s23d$ states to the two $6p_{1/2}nd$ and $6p_{3/2}nd$ series. For the high-n levels converging to the $6p_{1/2}$ limit we show only the envelope of the overlap integral corresponding to $\nu_2 = n_B + \frac{1}{2} + i$ where i is an integer, and for the $6p_{1/2}\epsilon d$ continuum we show the corresponding values of the overlap integral for the phase shifts $\pi\tau_2 = \pi\delta_2 = \pi(\delta_B \pm \frac{1}{2} + i)$. If $\tau_2 = \delta_2 = \delta_B$ the overlap integral

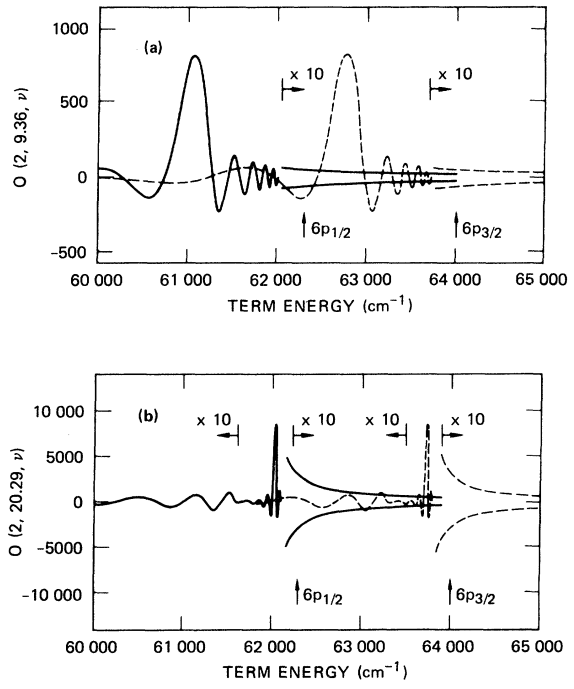

FIG. 12. Overlap integrals from (a) the Ba $6s12d$ state ($n_B = 9.36$) and (b) the $6s23d$ state ($n_B = 20.29$). In (a) the integral from $6s12d$ to the $6p_{1/2}nd$ channel (——) and $6p_{3/2}nd$ channel (— — —) are multiplied by 10 at 62 000 and 63 800 cm^{-1} as indicated. Note that the integrals extend smoothly across the $6p_{1/2}$ and $6p_{3/2}$ limits. Note also that the overlap integral peaks at ~61 000 and ~62 800 cm^{-1} near the $6p_{1/2}12d$ and $6p_{3/2}12d$ states. Maximum values are $(9.36)^3$, not 1, because of the normalization. In (b) the integral from $6s23d$ to the $6p_{1/2}nd$ channel (——) and $6p_{3/2}nd$ channel (— — —) are each multiplied by 10 in the energy ranges far from their peak values at 62 000 and 63 800 cm^{-1}, respectively.

to high-lying nd states converging to the $6p_{1/2}$ limit as well as to the continuum above the $6p_{1/2}$ limit vanishes by orthogonality. Our choice of the continuum phase shifts, $\pi\tau_2$, used in Fig. 12 yields the largest possible magnitudes of the overlap integral. Thus depending upon the actual phase shift $\pi\tau_2$, which must come out of the multichannel quantum-defect-theory analysis, the actual overlap integral lies between the positive and negative sides of the envelope of Fig. 12. The region near the $6p_{3/2}$ limit is plotted in an analogous fashion. Note that the overlap integral smoothly continues across the ionization limits. This is a consequence of our choice of the same phase for the high-n levels and the continuum waves and the fact that at small r the wave functions of these two are identical if the phase shift is the same.

From Fig. 12 we can see that there is a significant possibility of excitation to the continua just above the $6p_{1/2}$ and $6p_{3/2}$ limits. This is an interesting point since the lack of direct excitation to the continuum above the $6s_{1/2}$ limit where the energy of the free electron is $\gtrsim 2$ eV is one of the attractions of the multistep excitation scheme. We note though that in the case of the continua above the $6p_{1/2}$ and $6p_{3/2}$ limits the free electron has very low energy so that its wave function is somewhat similar to the wave function of the initial Rydberg state. An interesting example of this continuum excitation occurs just above the $6p_{1/2}$ limit in the vicinity of a $6p_{3/2}nd$ state. Figure 12 implies that in this region the dominant excitation from a high-lying $6snd$ state, such as $6s23d$, is to the $6p_{1/2}\epsilon d$ continuum not to the discrete $6p_{3/2}nd$ state.

In the usual configuration-interaction treatment pure continuum excitation in the vicinity of an autoionizing state corresponds to the Fano parameter $q=0$, in which case a symmetric decrease is observed in the photoexcitation cross section. However, this does not occur in the excitation from the $6s23d\,{}^1D_2$ state as shown in Fig. 13. The observed spectrum is peaked at the location of the $6p_{1/2}23d$ state, and the envelope falls off smoothly to higher and lower energy. Note, in particular, that the spectrum smoothly continues across the $6p_{1/2}$ limit showing evident enhancements at the locations of the $6p_{3/2}11d$

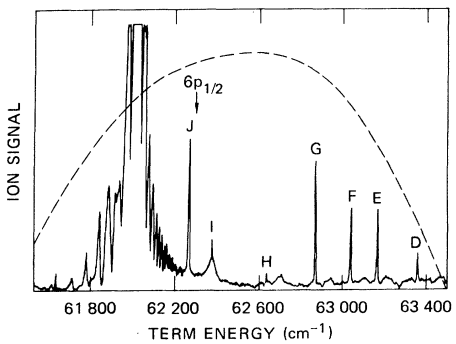

FIG. 13. Observed spectrum starting from the $6s23d\,{}^1D_2$ state to the region near the $(6p_{1/2}23d_{5/2})_{J=3}$ state. Note that the observed spectrum extends across the $6p_{1/2}$ limit and shows evident structure at the location of the $11d$ and $12d$ states converging to the $6p_{3/2}$ limit. Relative laser power is shown by the dashed curve.

and $6p_{3/2}12d$ states at 62 382 cm^{-1} and 62 707 cm^{-1} and then disappears. The fact that the spectrum above the $6p_{1/2}$ limit is a clear extension of the $6p_{1/2}nd$ series is an indication that the excitation is due to that channel. The fact that the signal does not increase at energies above 62 700 cm^{-1} indicates that the observed spectrum is not due to excitation to the $6p_{3/2}nd$ channel.

The fact that only the excitation of the $6p_{1/2}nd$ (ϵd) channel is important is supported by a three-channel quantum-defect treatment similar to those of Gounand *et al.*[9] and Lu.[15] As the calculations are a combination of the formal approach used in these two earlier papers and the physical insights of Sec. III we do not describe the calculations in any detail but simply define the parameters and present the results.

In this treatment we number the three collision, or i, channels as follows: channel 1, X continuum; channel 2, $6p_{1/2}nd_{5/2}$; channel 3, $6p_{3/2}nd_{3/2}$. The close-coupled, α, channels are numbered as follows: channel 1, Λ; channel 2, Ω; channel 3, Σ; and they have eigendefects of μ_1, μ_2, and μ_3. Here the labels Λ, Ω, and Σ serve to underscore the fact that the only observable role of the close-coupled channels is to couple the collision channels.

The unitary matrix $\underline{U}_{i\alpha}$ connecting the close-coupled and collision channels is given by a product of rotation matrices

$$\underline{U}_{i\alpha}=\underline{R}(\theta_{12})\underline{R}(\theta_{13})\underline{R}(\theta_{23}) , \tag{15}$$

where the $\underline{R}$ matrices are multiplied together in the order shown. $\underline{R}(\theta_{12})$, for example, is given by

$$\underline{R}(\theta_{12})=\begin{bmatrix} \cos\theta_{12} & \sin\theta_{12} & 0 \\ -\sin\theta_{12} & \cos\theta_{12} & 0 \\ 0 & 0 & 1 \end{bmatrix} . \tag{16}$$

To calculate the photoexcitation cross section corresponding to Fig. 13 we have used the quantum-defect parameters $\mu_1=0.31$, $\mu_2=0.27$, $\mu_3=0.61$, $\theta_{12}=0.20$, $\theta_{13}=0.87$, and $\theta_{23}=0.68$ (all angles are given in radians). In Fig. 14, we show the calculated photoexcitation cross section assuming excitation to either channel 2 or channel 3, and these results clearly show that just above the $6p_{1/2}$ limit the excitation to the $6p_{1/2}\epsilon d$ continuum (channel 2) is predominant.

Why the pure continuum excitation leads to an increase in the photoexcitation cross section at the location of the $6p_{3/2}11d$ state, for example, can be understood from the following two-channel picture. One of the factors in the excitation cross section is the overlap integral between $6s23d$ and the $6p_{1/2}\epsilon d$ continuum. Away from the $6p_{3/2}11d$ state the phase shifts of the $6p_{1/2}\epsilon d$ continuum and $6s23d$ state are nearly the same and thus the overlap integral is nearly zero by orthogonality. At the location of the $6p_{3/2}11d$ state the continuum undergoes a phase shift of π, necessarily producing a maximum in the overlap integral and thus the cross section, hence the enhanced structure observed in Fig. 13. In our three-channel model there are of course two open channels and two phase shifts which is why the calculated cross-section value assuming $6p_{1/2}\epsilon d$ excitation is neither as symmetric as one might expect nor does it go to zero away from the location of the $6p_{3/2}nd$ states (see Fig. 14). Nevertheless, it is clear that the observed spectral feature arises from the continuum excitation alone and is quite different from what would be expected if we were exciting the atoms from the ground state.

As implied by Fig. 12 the excitations from the $6s23d\,^1D_2$ state to the $6p_{1/2}nd$ and $6p_{3/2}nd$ channels are localized near the $6p_{1/2}23d$ and $6p_{3/2}23d$ states, respectively, and they do not overlap significantly. For excitations from lower-lying states such as $6s12d\,^1D_2$ there is substantial overlap of the excitation amplitudes to the $6p_{1/2}nd$ and $6p_{3/2}nd$ channels, and there is possibility of interferences. However, as the overlap occurs in a perturbed region of the spectrum, it is impossible to separate the two effects with confidence.

As shown in Sec. III, the observed spectra are very sensitive to perturbations of the regularity of autoionizing series, and as a result any perturbation of a series of autoionizing states stands out quite clearly. A good example is the perturbation of the Ba $6p_{1/2}nd$ series at $n=20$ by the $6p_{3/2}10d$ state. The effects of the perturbation are two: to change the quantum defects of the $6p_{1/2}nd_{5/2}$ states and to alter their widths in the vicinity of $n=20$. In Fig. 15 we show the observed spectrum from the $6s22d$ state in which the irregularity at $n=20$ is very apparent, as expected. The excitation to the $6p_{3/2}nd$ channel is negligible as can be inferred immediately from Fig. 12, the plot of the overlap integrals, thus in calculating the

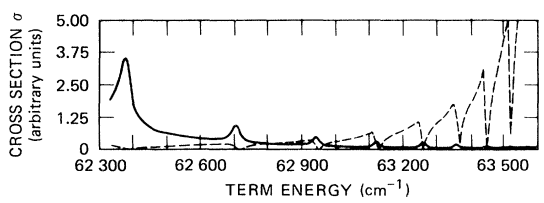

FIG. 14. Calculated cross sections σ for the excitation from the $6s23d$ state to the energy range (above the $6p_{1/2}$ limit) shown in Fig. 13 assuming only channel 2 (——) and only channel 3 excitation (— — —).

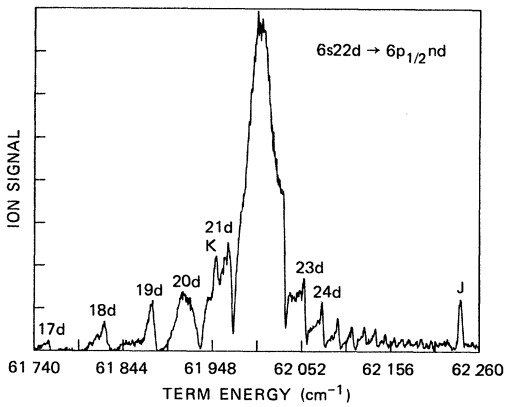

FIG. 15. Observed spectrum from the Ba $6s22d\,^1D_2$ state to the perturbed region near $(6p_{1/2}20d_{5/2})_{J=3}$.

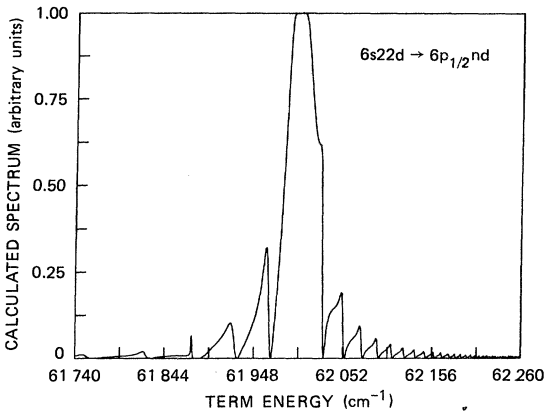

FIG. 16. Calculated spectrum from the Ba $6s22d\,^1D_2$ state to the perturbed region near $(6p_{1/2}20d_{5/2})_{J=3}$.

spectrum of Fig. 15 we can to a good approximation consider only the excitation to the $6p_{1/2}nd$ channel. Accounting for the saturation (or depletion broadening) by the high laser powers as in Eq. (1) leads to the calculated spectrum shown in Fig. 16. The choice of quantum-defect parameters, $\mu_1=0.20$, $\mu_2=0.81$, $\mu_3=0.74$, $\theta_{12}=0.47$, $\theta_{13}=0.20$, and $\theta_{23}=0.83$ (all angles in radians), is a compromise in that it accounts reasonably well for the interaction between the $6p_{1/2}nd$ and $6p_{3/2}nd$ series and gives reasonable values for the $6p_{1/2}nd$ positions, but understates their widths. In spite of this difficulty, which is a direct consequence of including only one continuum, we are able to reproduce the experimental spectrum of Fig. 15 reasonably well.

V. CONCLUSION

We have described the multistep laser excitation of autoionizing Rydberg states under the condition where the final transition is driven by a laser with enough power to bring out very weak features of the spectrum. Using a simple quantum-defect-theory treatment to extend the physical interpretation initially advanced to explain observed low-power spectra we have shown that the observed spectra can be understood as arising from the product of the spectral density of the series of autoionizing states and the overlap integral with the initial state. Not surprisingly, the weak features visible in these high-power spectra present some rather interesting effects. For example, in such spectra perturbations of series of autoionizing states stand out very clearly, and a pure continuum absorption is observed which is different from that expected on the basis of the more conventional configuration-interaction treatment.[2]

Several applications to take advantage of the understanding of these high-power spectra appear promising. We have here shown that this is an excellent method for detecting local perturbations in an autoionizing Rydberg series. In addition, we have observed that mixing between two channels converging to the same limit can be studied using this technique. Finally, we note that to reach Ba autoionizing states converging to higher core states of Ba^+ from the bound Rydberg states two-photon excitation through one of the lower channels of autoionizing states has been shown to be useful.[16] In general, such schemes lead to single-photon ionization and the consequent loss of two-photon signal. However, if we tune the first laser to one of the overlap-integral zeros we may avoid one-photon excitation while still having a small detuning between the real and virtual intermediate states, preserving a large two-photon amplitude. Such a technique has been shown to be viable[17] and may prove to be quite useful in future experiments.

ACKNOWLEDGMENTS

This work was supported by the National Science Foundation under Grant No. PHY-83-06082. It is a pleasure to acknowledge helpful comments from U. Fano, W. E. Cooke, and A. P. Hickman.

*Permanent address: Laboratoire Aimé Cotton, Centre National de la Recherche Scientifique, Campus d'Orsay, F-91405 Orsay Cedex, France.

[1]W. E. Cooke, T. F. Gallagher, S. A. Edelstein, and R. M. Hill, Phys. Rev. Lett. 40, 178 (1978).
[2]U. Fano, Phys. Rev. 124, 1866 (1961).
[3]W. E. Cooke, S. A. Bhatti, and C. L. Cromer, Opt. Lett. 7, 69 (1982).
[4]N. H. Tran, R. Kachru, and T. F. Gallagher, Phys. Rev. A 26, 3016 (1982).
[5]C. E. Moore, *Atomic Energy Levels*, U.S. Natl. Bur. Stand. Circular No. 467 (U.S. GPO, Washington, D.C., 1949).
[6]J. R. Rubbmark, S. A. Borgström, and K. Bockasten, J. Phys. B 10, 421 (1977).
[7]U. Fano, Phys. Rev. A 2, 353 (1970).
[8]K. T. Lu and U. Fano, Phys. Rev. A 2, 81 (1970).
[9]F. Gounand, T. F. Gallagher, W. Sandner, K. A. Safinya, and R. Kachru, Phys. Rev. A 27, 1925 (1983).
[10]W. E. Cooke (unpublished).
[11]S. A. Bhatti, C. L. Cromer, and W. E. Cooke, Phys. Rev. A 24, 161 (1981).
[12]M. L. Zimmerman, M. G. Littman, M. M. Kash, and D. Kleppner, Phys. Rev. A 20, 2251 (1979).
[13]H. A. Bethe and E. A. Salpeter, *Quantum Mechanics of One and Two Electron Atoms* (Academic, New York, 1957).
[14]A. Lindgard and W. E. Nielsen, At. Data Nucl. Data Tables 19, 534 (1977).
[15]K. T. Lu, Phys. Rev. A 4, 579 (1971).
[16]R. M. Jopson, R. R. Freeman, W. E. Cooke, and J. Bokor, Phys. Rev. Lett. 51, 1640 (1983).
[17]T. F. Gallagher, R. Kachru, N. H. Tran, and H. B. van Linden van den Heuvell, Phys. Rev. Lett. 51, 1753 (1983).